INTERNATIONAL JOURNAL FOR NUMERICAL AND ANALYTICAL METHODS IN GEOMECHANICS
Int. J. Numer. Anal. Meth. Geomech. (2016)
Published online in Wiley Online Library (wileyonlinelibrary.com). DOI: 10.1002/nag.2498

On the stability of fissured slopes subject to seismic action

S. Utili[1,*,†] and A.H. Abd[1,2]

[1]*School of Engineering, University of Warwick, CV4 7AL Coventry, U.K.*
[2]*Civil Engineering Department, College of Engineering, Tikrit University, Tikrit, Iraq*

SUMMARY

A set of analytical solutions achieved by the upper bound theorem of limit analysis and the pseudo-static approach is presented for the assessment of the stability of homogeneous c, ϕ slopes manifesting vertical cracks and subject to seismic action. Rotational failure mechanisms are considered for slopes with cracks of either known or unknown depth and location. A validation exercise was carried out based on numerical limit analyses and displacement-based finite-element analyses with strength reduction technique.

Charts providing the stability factor for fissured slopes subject to both horizontal and vertical accelerations for any combination of c, ϕ and slope inclination are provided. The effect of the direction of the vertical acceleration on slope stability is specifically analysed. Yield seismic coefficients are also provided.

When the presence of cracks within the slope can be ascertained with reasonable confidence, maps showing the zones within the slope where they have no destabilising effect are provided.

Finally, Newmark's method was employed to assess the effect of cracks on earthquake induced displacements. To this end, displacement coefficients are provided in chart form as a function of the slope characteristics. Two examples of slopes subjected to known earthquakes are illustrated.

Received 27 February 2015; Revised 17 September 2015; Accepted 10 December 2015

KEY WORDS: limit analysis; upper bound; kinematic approach; crack; earthquake; stability chart; landslide

1. INTRODUCTION

The presence of cracks or fissures in slopes made of cohesive soils (e.g. clayey soils) and/or rock because of the development of tension for instance has long been recognised as an important factor affecting their stability since the time of Terzaghi [1]. The presence of cracks poses significant challenges to the assessment of slope stability because they introduce one or a few discontinuities that may substantially reduce the stability of the slope. In the case of a small number of discontinuities, homogenisation techniques work badly because the slope behaviour tends to be heavily affected by the specific features of each discontinuity that therefore has to be considered explicitly in the stability analysis of the slope. This implies a significant extra computational effort for the numerical methods typically used in continuum mechanics (e.g. finite element (FE) method, finite difference method, etc.) that struggle to include discrete discontinuities. Furthermore, if a comprehensive parametric analysis is to be run to explore how slope stability is affected by the presence of cracks for a variety of geometrical and mechanical parameters of the slope, the computational effort required appears prohibitive. Hence, the appeal of an analytical solution is apparent.

In the large body of literature on limit analysis applied to slopes subject to seismic excitation (e.g. [2–9]), there is no provision to take into account the presence of cracks. In this paper, an analytical method based on

*Correspondence to: S. Utili, School of Engineering, University of Warwick, CV4 7AL Coventry, U.K.
†E-mail: s.utili@warwick.ac.uk

the upper bound theorem of limit analysis and on the so-called pseudo-static approach [10] is presented for the assessment of the stability of uniform c, ϕ slopes manifesting vertical cracks and subject to seismic action.

Three situations are considered in this paper:

i) the most unfavourable scenario of cracks present in the slope (such a scenario may be assumed by practitioners in the absence of reliable information on the presence of cracks);
ii) slopes subject to cracks of known depth;
iii) slopes subject to cracks of known location.

With regard to the first problem, *i*), the assumption of the most unfavourable scenario reflects the fact that often neither the position nor the depth of a crack are known. In this case, all possible failure mechanisms involving any crack that may be present in the slope must be considered in the analysis. Assuming the terminology of Terzaghi [1], Taylor [11] and Chen [12], the 'stability factor' for a slope at impending failure is defined as $N_s = \gamma H_{cr}/c$, with γ being the ground unit weight, H_{cr} the critical slope height and c the ground cohesion (note that in some references the stability factor may be called stability number). On the basis of the obtained solutions, charts of (least upper bound) stability factor versus inclination of the slope face, β, are presented in the paper for all values of engineering interest of internal friction angle, ϕ, and horizontal and vertical seismic coefficients, K_h and K_v respectively. These charts, together with the values reported in tabular form in the 'Supporting Information', can be used by practitioners to get an immediate estimate of the destabilising influence of the presence of cracks on the slope of interest for any level of prescribed seismic action.

However, if reliable information on the cracks existing in the slope is available, the conservative assumption of the most unfavourable scenario is no longer justified. In this eventuality, either the depths of the cracks (problem *ii*) or their locations (problem *iii*) can be prescribed reducing the number of potential failure mechanisms to be considered in the search for the least upper bound. With regard to crack depth, according to some lower bound analyses (e.g. [1, 13, 14]), it can be determined as a function of the tensile strength of the ground and its stress state. However, exceedance of the ground tensile strength is only one of the possible causes for the formation of cracks, because there is experimental evidence about cracks caused and/or deepened by processes such as the occurrence of differential settlements [15], desiccation [16–20] and freezing [21]. In the large majority of cases, accurate estimates of crack depths are not available to the practitioner; therefore, the stability of a slope needs to be analysed for a range of possible crack depths rather than a single value. Accordingly in the paper, the yield horizontal acceleration is calculated for various prescribed crack depths.

Numerical simulations with other methods, namely FE limit analysis (numerical upper and lower bounds) and FE displacement based method with strength reduction technique, were run to validate the obtained results. A very good agreement in terms of both geometry of the predicted failure mechanism and yield seismic coefficient was found.

Then, an analysis of the influence of the vertical seismic acceleration on slope stability is presented for both cases of intact and fissured slopes. Dimensionless charts showing which case is more critical for the stability of slopes between no vertical acceleration, upward acceleration and downward acceleration are provided for any combination of β, ϕ and K_h. Also, maps showing zones where cracks have no detrimental effect on slope stability are provided for various combinations of horizontal and vertical accelerations. To this end, the locations of the cracks (problem *iii*) are prescribed in the search for the most unfavourable failure mechanism. These maps can be employed for two purposes: (*i*) in the case of earth structures prone to fissuring, as for instance flood defence embankments [17, 20, 22, 23], they may help inspection engineers to reduce significantly the extension of the zones to be inspected by excluding the zones where cracks have no detrimental effect on slope stability; (*ii*) when the presence of one or more cracks in a slope is known, the maps tell the geotechnical engineer whether the crack may be discarded from the stability analysis of the slope.

Finally, Newmark's approach [24], also called 'block sliding procedure', was used to calculate seismic induced displacements. Horizontal yield accelerations were calculated for any combination of values of β, ϕ, λ and of the normalised cohesion, $\frac{c}{\gamma H}$, of engineering interest, having assumed the presence of the most unfavourable crack in the slope. In the analysis here presented, unlike Newmark's original formulation which assumes translational failure mechanisms, rotational mechanisms were used instead because they are more critical for the stability of slopes. Seismic displacement coefficients were calculated as a

DOI: 10.1002/nag

function of slope characteristics (ϕ and β values). Finally, the influence of crack depth on earthquake induced displacements was investigated.

2. DERIVATION OF THE ANALYTICAL SOLUTION

The failure mechanisms assumed in our analysis are 2D single wedge rigid rotational mechanisms (see Figure 1). The failing wedge E-D-C-B rigidly rotates around point P with the ground lying on the right of the log-spiral D-C and of the vertical crack C-B remaining at rest. The equation of the log-spiral D-C is:

$$r = r_\chi \exp[\tan\phi(\theta - \chi)] \tag{1}$$

with r being the distance of a generic point of the spiral to its centre, θ being the angle formed by r with the horizontal axis, r_χ identifying the distance of point F of the spiral to its centre and χ being the angle made by segment P-F with the horizontal (see Figure 1).

The upper bound is derived by imposing energy balance for the failing wedge E-D-C-B:

$$\dot{W}_d = \dot{W}_{ext} \tag{2}$$

where $\dot{W}_d$ and $\dot{W}_{ext}$ are the rate of dissipated energy and of external work respectively. The calculation of $\dot{W}_d$ accounting for the energy dissipated along the log-spiral segment D-C is reported in [25]. Note that in this formulation cracks are treated as no-tension non-cohesive perfectly smooth (no friction) interfaces; therefore, no energy is ever dissipated along a crack and the angle η is $0° < \eta < 180°$. Michalowski [26] has provided a limit analysis upper bound formulation for vertical cracks that are absent prior to the formation of the failure mechanism but instead form simultaneously with the onset of the failure mechanism in an initially intact slope because of the soil tensile strength being exceeded at the same time as the log-spiral surface D-C is formed. However, cracks generated as part of the failure mechanism taking place are always less detrimental (critical) to slope stability than cracks pre-existing the formation of the slope failure mechanism, because they require energy to be dissipated for their formation which instead is not the case for pre-existing cracks [26]. Therefore, in this paper only the presence of (more critical) pre-existing cracks is considered.

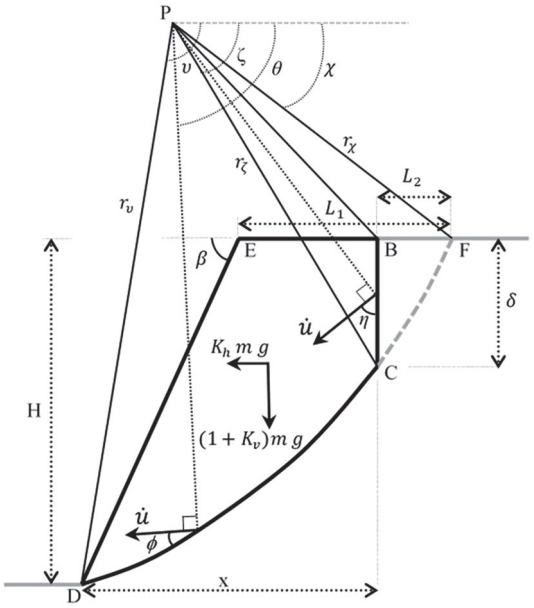

Figure 1. Failure mechanism. Note that $\eta \neq \phi$. The wedge of soil enclosed by black lines D-C (logarithmic spiral failure line), B-C (pre-existing crack), B-E (upper surface of the slope) and E-D (slope face) rotates around point P.

DOI: 10.1002/nag

The rate of external work for the sliding wedge E-B-C-D, $\dot{W}_{ext}$, is calculated as the work of block E-D-F minus the work of block B-C-F. The work of block E-D-F is calculated by algebraic summation of the work of blocks P-D-F, P-E-F and P-D-E [12]. The work of block B-C-F is calculated by algebraic summation of the work of blocks P-C-F, P-B-F and P-C-B [25, 27, 28]. Note that here, in addition to the weight force, a horizontal pseudo-static force, $F_{PSh}=mK_{h}g=\gamma K_{h}A$ (g being the gravitational acceleration, m the mass of the wedge and A its area), and a vertical one, $F_{PSv}=mK_{v}g=\gamma K_{v}A$, are added to account for the seismic action [3, 4].

The calculation of the expressions for $\dot{W}_{ext}$ for each block is provided in Appendix A. Substituting them into Eq. (2), the following is obtained:

$$c\dot{\theta}r_{\chi}^{2}f_{d}=\dot{\theta}\gamma r_{\chi}^{3}\left[\begin{array}{c}(1+K_{v})(f_{1v}-f_{2v}-f_{3v}-f_{4v}+f_{5v}+f_{6v})+\\ K_{h}(f_{1h}-f_{2h}-f_{3h}-f_{4h}+f_{5h}+f_{6h})\end{array}\right] \tag{3}$$

with $f_{1v}, f_{2v}, \ldots f_{6h}$ provided in Appendix A and f_d provided in [25]. Dividing all terms in Eq. (3) by $\dot{\theta}$ and r_{χ}^{2}, and rearranging, the upper bound on the stability factor, $N=\gamma H/c$, is obtained:

$$N=\frac{\gamma H}{c}=f(\chi,\upsilon,\zeta,\phi,\beta,K_{h},\lambda)=\frac{f_{d}[\exp[\tan\phi(\upsilon-\chi)]\sin\upsilon-\sin\chi]}{\left[\begin{array}{c}(1+\lambda K_{h})(f_{1v}-f_{2v}-f_{3v}-f_{4v}+f_{5v}+f_{6v})+\\ K_{h}(f_{1h}-f_{2h}-f_{3h}-f_{4h}+f_{5h}+f_{6h})\end{array}\right]} \tag{4}$$

with $\lambda=K_{v}/K_{h}$ (consistent with Figure 1, the + sign indicates vertical downward acceleration, whereas the − sign indicates vertical upward acceleration). The global minimum of $f(\chi, \upsilon, \zeta, \phi, \beta, K_{h}, \lambda)$ over the three geometrical variables χ, υ, ζ provides the least (best) upper bound on the stability factor having assumed that the most unfavourable crack for the slope is present.

By solving Eq. (3) with respect to K_{h} instead, the upper bound on the yield seismic coefficient, K_y, is obtained:

$$\begin{aligned}K_{y}&=f_{y}(\chi,\upsilon,\zeta,\phi,\beta,c/\gamma H,\lambda)\\&=\frac{(c/\gamma H)f_{d}[\exp[\tan\phi(\upsilon-\chi)]\sin\upsilon-\sin\chi]-(f_{1v}-f_{2v}-f_{3v}-f_{4v}+f_{5v}+f_{6v})}{\lambda(f_{1v}-f_{2v}-f_{3v}-f_{4v}+f_{5v}+f_{6v})+(f_{1h}-f_{2h}-f_{3h}-f_{4h}+f_{5h}+f_{6h})}.\end{aligned} \tag{5}$$

The global minimum of $f_{y}(\chi,\upsilon,\zeta,\phi,\beta,c/\gamma H,\lambda)$ over the three geometrical variables χ,υ,ζ provides the least (best) upper bound on K_y.

Note that unlike the case of intact slopes, here failure mechanisms may in principle daylight on the slope face above the slope toe. Hence potential failure mechanisms passing above the toe were considered in our analysis by discretising the slope face in several points and calculating the stability factor associated to each potential mechanism (see Figure 2a). In all the cases considered here no potential mechanism passing above the slope toe turned out to be a failure mechanism.

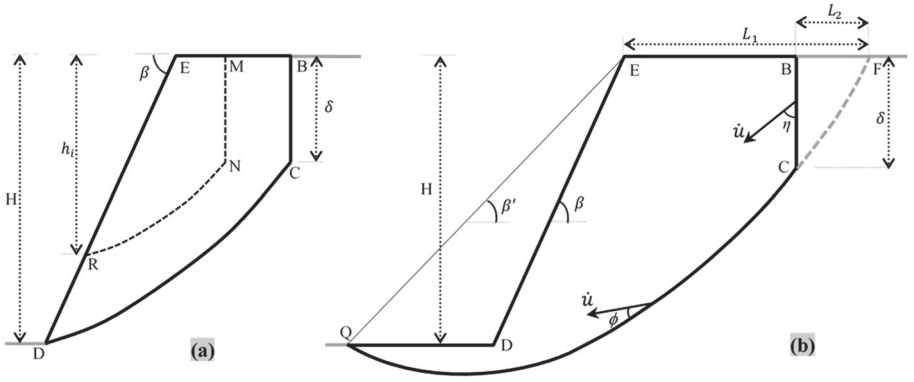

Figure 2. a) Potential failure mechanism passing above the slope toe (wedge E-R-N-M) and the one taking place (wedge E-D-C-B),(after [25]). b) Failure mechanism passing below the slope toe (wedge E-D-Q-C-B).

DOI: 10.1002/nag

In the case of intact slopes with a low value of ϕ, [9] found that for high values of K_h, the failure mechanism passes below the slope toe (see Figure 2b). The results reported here in our paper include both types of failures. Failure mechanisms passing below the toe were found for slopes with low friction (e.g. $\phi = 20°$) and high $c/\gamma H$ (see Figure 8a).

3. STABILITY FACTOR

The global unconstrained minimization of $f(\chi, \upsilon, \zeta, \phi, \beta, K_h, \lambda)$ in Eq. (4) provides the best upper bound on the slope stability factor when the most unfavourable crack is present. The obtained upper bounds are plotted in Figure 3 against the inclination of the slope face, β, for $\phi = 20°$, 30° and 40°, with K_h ranging from 0.1 to 0.4, and for λ ranging from −1 to +1. For sake of completeness, the largest range of λ reported in the literature (λ ranging from −1 to +1) was chosen (see [29] and [30]). The four charts of Figure 3 are useful to practitioners in order to get an immediate estimate, erring on the safe side, of the stability of a fissured slope subject to seismic excitation when no data on either the depth or the position of the existing cracks are known. For some combinations of the slope parameters, a translational failure mechanism, indicated by grey lines in the figures, occurs instead of the rotational one. Note that translational mechanisms are always particular cases of rotational ones, obtained when the radius of the spiral, r_χ, approaches infinity.

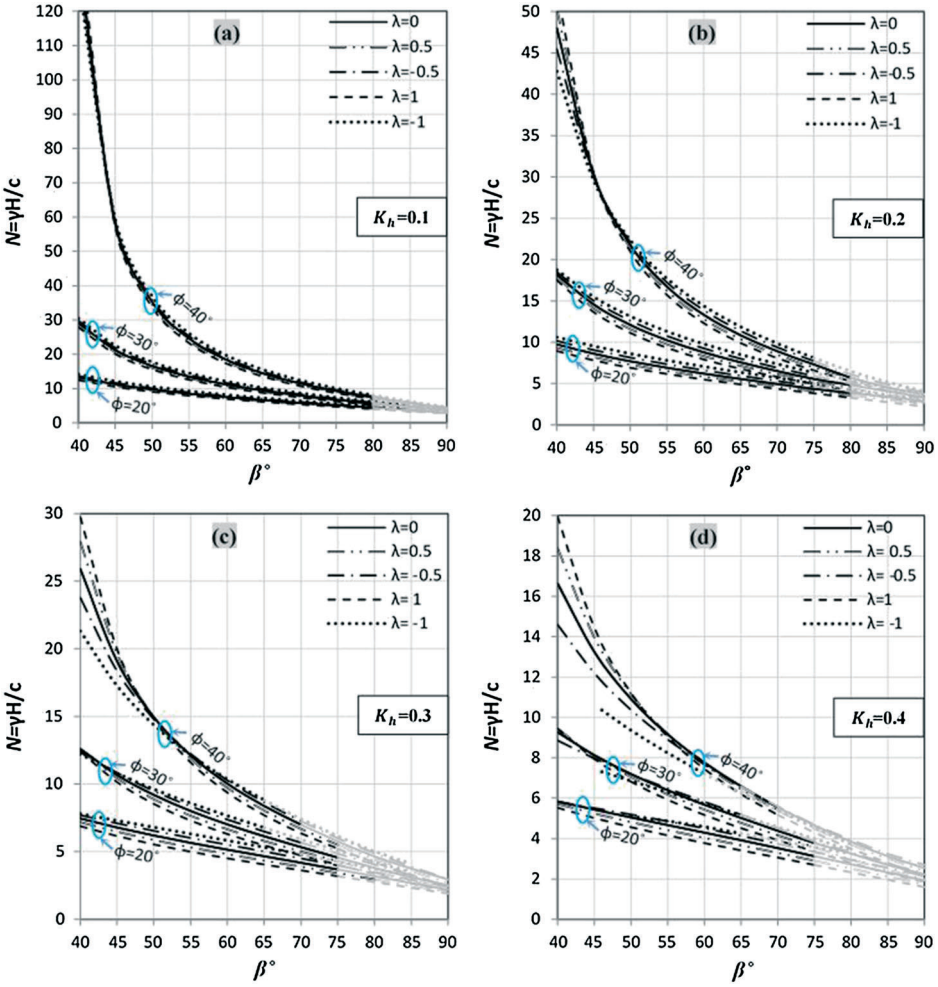

Figure 3. Stability factor against slope inclination for the most unfavourable crack scenario, i.e. the most critical mechanism among all the potential mechanisms involving cracks of any depth and location is sought, with $\lambda = K_v/K_h$. a) $K_h = 0.1$; b) $K_h = 0.2$; c) $K_h = 0.3$ and d) $K_h = 0.4$. Grey lines indicate the cases where the log-spiral failure surface (rotational failure mechanism) degenerates into a plane (translational failure mechanism).

DOI: 10.1002/nag

A key question from a practitioner's viewpoint is how much the presence of cracks may affect slope stability and when they may be safely neglected in a stability analysis. The answer to this is provided in Figure 4, where the difference in percent between the obtained stability factors and the corresponding factors for a slope of the same characteristics but intact is plotted for all the parameter combinations of engineering interest. From the figure is apparent that the presence of cracks can cause substantial reduction of stability (up to 30%), with the reduction being more significant for steep slopes. This result is explained by the fact that steep slopes are subject to failure mechanisms that involve deeper cracks than gentle slopes. The depth, δ_c, and location, x_c, of the crack associated to the failure mechanism found as a result of the analysis for various levels of K_h are plotted in Figure 5a and 5b respectively. The subscript 'c' stands for critical because the crack here considered is the most critical that may exist for the stability of the slope. From the figure emerges that δ_c increases with K_h whatever the slope inclination. Also for $\beta \to 90°$, $x_c \to 0$ independently of the value of K_h. In Figure 5b, the horizontal distance of the crack from the slope crest, x_c, is plotted against β. It turns out that the higher the intensity of the seismic excitation, the more x_c shifts inwards. When $\beta \to 90°$, $x_c \to 0$ independently of the level of K_h with the failing wedge becoming an infinitesimal slice. As observed in Utili [25] in the absence of seismic action, $\beta = 90°$ is a singular case with the failure mechanism involving a vertical slice of infinitesimal width and of finite height H, translating away ($r_\chi \to \infty$). Finally comparing the curves plotted in Figure 4 for different levels of K_h, it can be inferred that the stronger the earthquake is, the larger the reduction of slope stability caused by the presence of cracks. On the other hand when β is close to ϕ and K_h is small, the reduction of N is

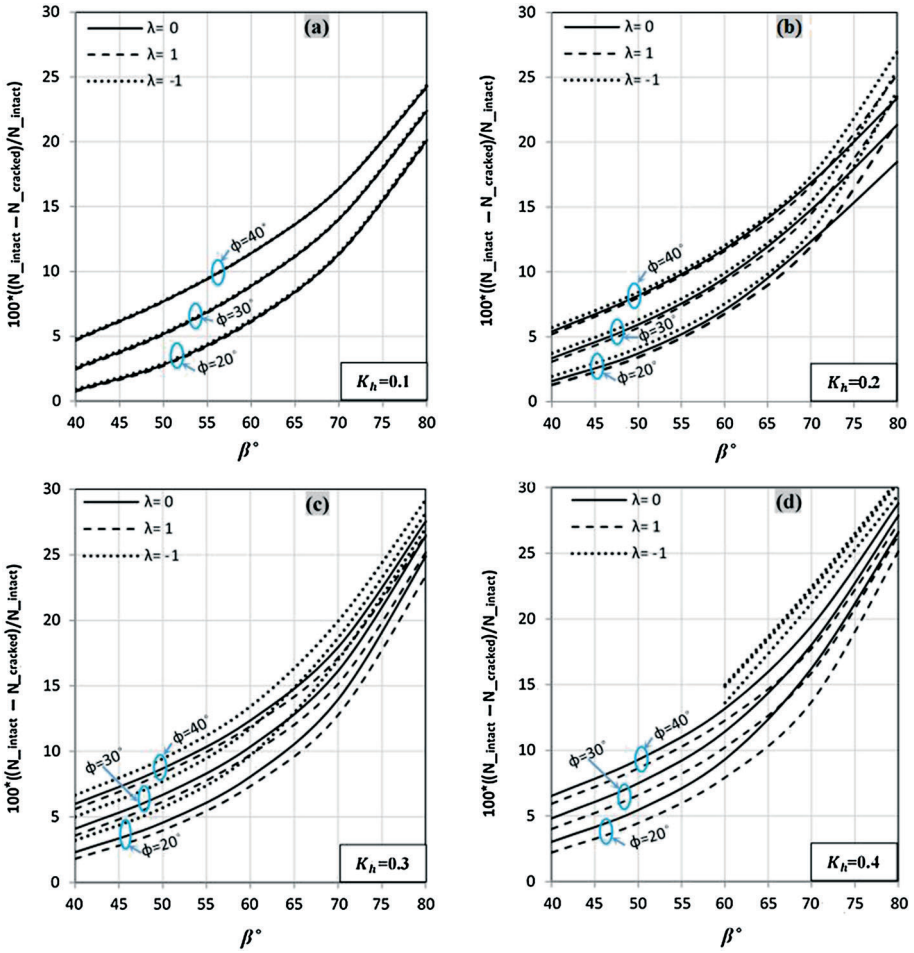

Figure 4. Reduction in percent of the stability factor due to the most unfavourable crack versus slope inclination, for various combinations of ϕ, K_h and λ.

DOI: 10.1002/nag

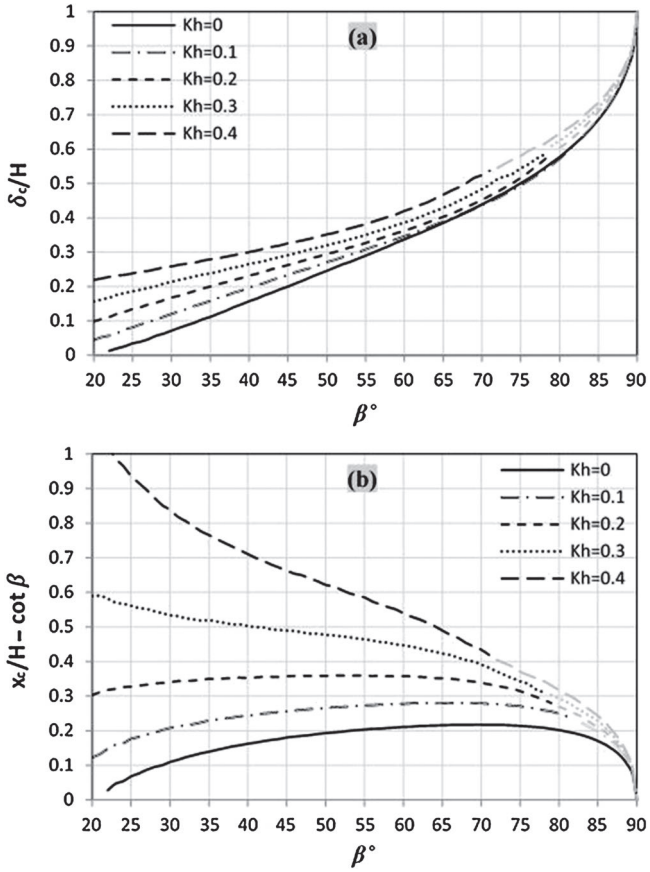

Figure 5. a) Depth of the most unfavourable crack versus slope inclination for various K_h with $\phi = 20°$ and $\lambda = 0$. b) Location of the most unfavourable crack, measured from the slope toe, versus slope inclination for various K_h with $\phi = 20°$ and $\lambda = 0$. Black curves indicate a rotational failure mechanism, whilst grey curves indicate a translational failure mechanism.

less than 5%. So it can be concluded that the presence of cracks cannot be neglected but in the case of gentle slopes of high internal friction angle subject to moderate earthquakes.

In previous limit analysis works accounting for the presence of a vertical pseudo-static acceleration, this is always assumed to be downward (e.g. [4, 29]) implying that downward acceleration is always detrimental to slope stability whereas upward acceleration is beneficial or, at least less detrimental than the downward one. Here instead, it will be shown that both downward and upward directions can be detrimental (or beneficial) depending on the geometrical and mechanical characteristics of the slope. As shown in Figure 3, in general the stability factor increases with the value of λ (with the lowest line being for $\lambda = +1$ and the highest one for $\lambda = -1$), so for low values of ϕ, downward vertical acceleration is detrimental to stability whereas upward acceleration is beneficial. This is in agreement with the assumption routinely made in the literature. However, examining the charts of Figure 3 more closely, there are several instances where curves for the same ϕ and K_h but different λ value intersect. For instance all the lines obtained for $K_h = 0.2$ and $\phi = 40°$ intersect at $\beta \approx 47°$ (see Figure 3b): on the right side of the intersection point, N decreases with λ increasing, but on the left side of the point, the trend is the opposite with N increasing for λ increasing. So on the left side of $\beta = 47°$, upward vertical acceleration is detrimental to slope stability whereas downward acceleration is beneficial. This trend becomes increasingly more marked for higher K_h. The results here illustrated are in agreement with the analysis recently carried out by Shukha and Baker [30] employing limit equilibrium on intact slopes; however, the results here illustrated were obtained for slopes subject to cracks and are based on the rigorous framework of limit analysis.

At high values of K_h (see chart 3c and 3d), there are several intersection points between the curves obtained for the same ϕ and K_h values rather than one. This makes it difficult to establish which case is

DOI: 10.1002/nag

more critical. To address this question, the maps of Figure 6 are provided. In the maps, four zones exist. In zone 1, the stability factor for vertical downward acceleration, $N_{\downarrow}$, is lower than the factor for the case of no vertical acceleration, N_0, that in turn is lower than the factor for the case of vertical upward acceleration, $N_{\uparrow}$. In zone 2 $N_{\uparrow} < N_{\downarrow} < N_0$, in zone 3 $N_{\downarrow} < N_{\uparrow} < N_0$ and in zone 4 $N_{\downarrow} < N_0 < N_{\uparrow}$. The four zones exist for intact slopes as well (see Figure 6b and 6d). Comparing the maps obtained for fissured slopes with the ones obtained for the corresponding intact slopes subject to the same λ values (i.e. Figure 6a with 6b and Figure 6c with 6d), it turns out that the presence of cracks makes zones 2 and 3 larger. Another observation can be made about the influence of the magnitude of K_v on the extension of those zones. Comparing Figure 6a with 6c and Figure 6b with 6d it is apparent that the higher the value of $|\lambda|$ (hence the higher the value of K_v) the larger the extension of the zones is.

In Figure 7a, the boundary between the zone where $N_{\uparrow} < N_{\downarrow}$ and where $N_{\downarrow} < N_{\uparrow}$ is plotted for various levels of K_h and λ. This figure provides the key information needed by practitioners to decide whether to assume upward or downward vertical acceleration for the stability analysis of a given slope. For sake of completeness also the boundary between the zone where $N_0 < N_{\downarrow}$and $N_{\downarrow} < N_0$ is plotted in Figure 7b and the boundary between the zone where $N_{\uparrow} < N_0$ and $N_0 < N_{\uparrow}$ in Figure 7c.

4. YIELD SEISMIC COEFFICIENT

The yield (in some references also called critical) horizontal acceleration, gK_y, is a key parameter informing practitioners of the level of seismic acceleration for which a given slope, stable under static conditions, becomes unstable. Also, it is needed to calculate earthquake induced permanent displacements via the Newmark's approach [24].

The global minimum of $f_y(\chi, \upsilon, \zeta, \phi, \beta, c/\gamma H, \lambda)$ over the three geometrical variables χ, υ, ζ (see Eq. (5)) provides the least upper bound on the yield seismic coefficient, $K_{y,}$ assuming that the most unfavourable

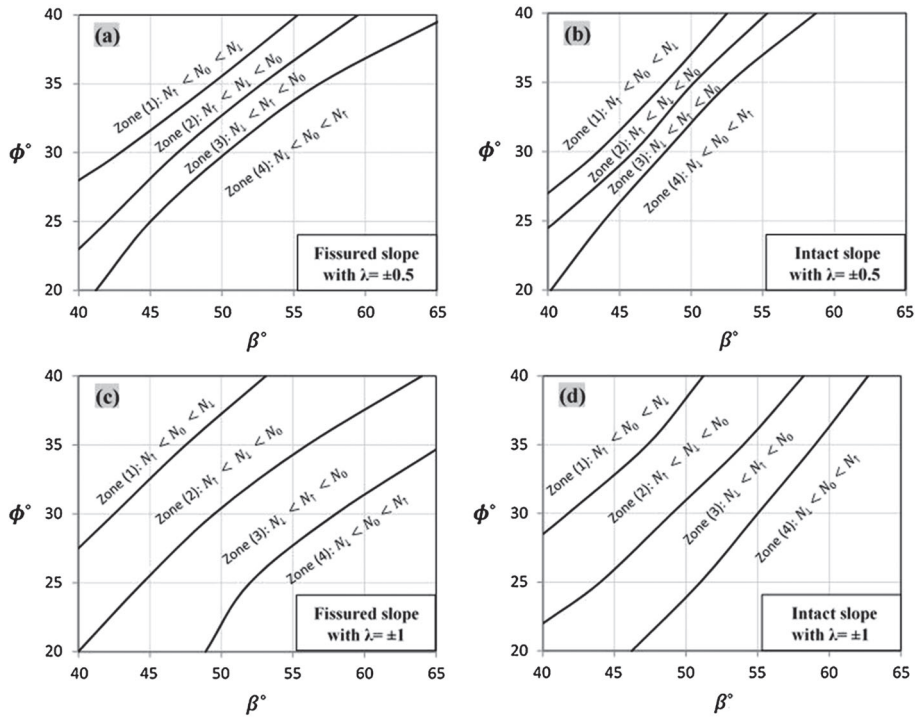

Figure 6. Charts illustrating which case is more critical for various combinations of ϕ and β with $K_h = 0.4$. $N_{\uparrow}$, N_0 and $N_{\downarrow}$ represent the stability numbers ($\gamma H/c$) calculated considering upward vertical acceleration, zero vertical acceleration and downward vertical acceleration respectively.

DOI: 10.1002/nag

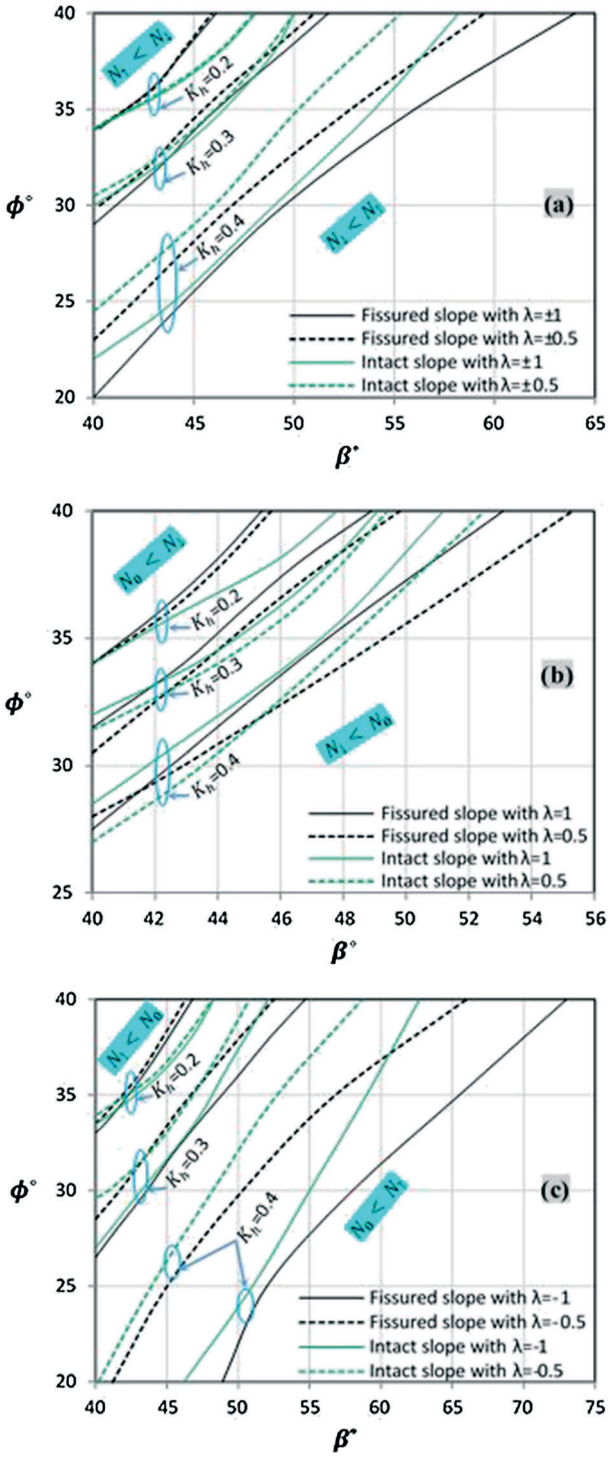

Figure 7. Black lines are for fissured slopes (most unfavourable crack scenario), coloured lines for intact slopes. a) in the region above the lines, $N_\uparrow < N_\downarrow$; the opposite holds true in the region below; b) in the region above the lines, $N_0 < N_\downarrow$; the opposite holds true in the region below; c) in the region above the lines, $N_\uparrow < N_0$; the opposite holds true in the region below.

crack for the slope is present. In Figure 8, the obtained upper bounds are plotted for slopes of various characteristics (β, ϕ, $c/\gamma H$) together with the upper bounds obtained for intact slopes. In Figure 9 the difference in percent between the obtained yield seismic coefficients and the corresponding coefficients

DOI: 10.1002/nag

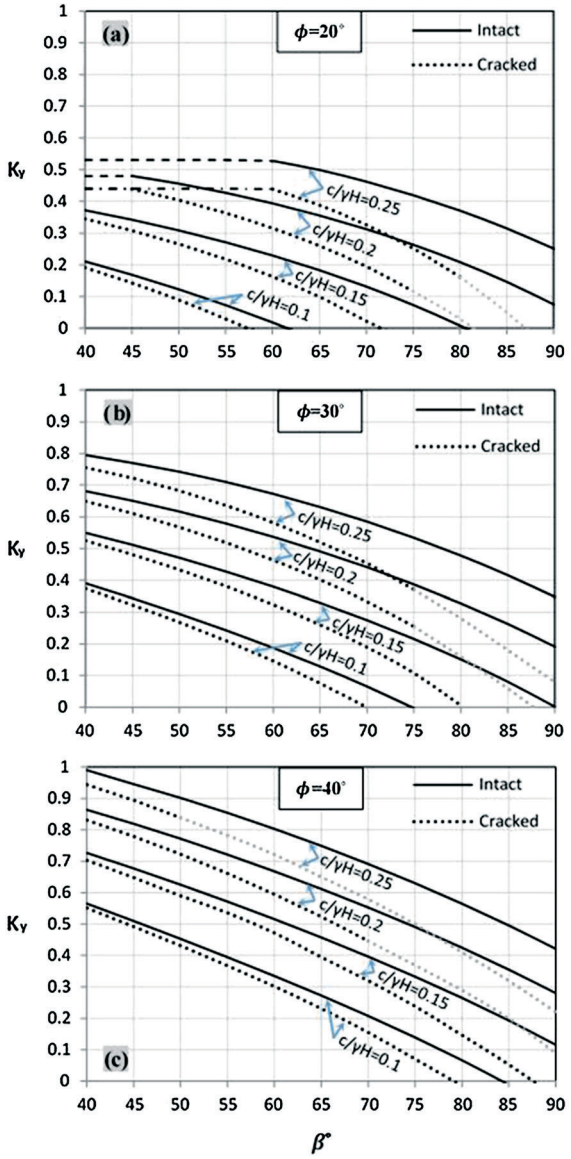

Figure 8. Coefficient of yield acceleration versus slope inclination for intact slopes (solid lines) and for fissured slopes for the most unfavourable crack scenario (dotted lines), i.e. the most critical mechanism among all the potential mechanisms involving cracks of any depth and location is sought. Vertical acceleration is absent ($\lambda = 0$): a)) $\phi = 20°$; b)) $\phi = 30°$; c)) $\phi = 40°$. Grey lines indicate a translational failure mechanism. Dashed and dashed-dotted lines indicate a below the slope toe mechanism occurring for intact and fissured slopes respectively.

for a slope of the same characteristics but intact is plotted. It can be seen that the presence of cracks causes substantial reduction of the yield seismic coefficient, especially for steep slopes of low ϕ. This result is in agreement with the trend observed in Figure 4 for the reduction of the stability factor under a prescribed gK_h. Figure 9 is useful to investigate the relative influence between the two ground strength parameters (c and ϕ) on the yield seismic coefficient. Looking at the charts for $\beta = 60°$ and $\beta = 75°$ (see Figures 9b and 9c respectively) it can be noticed that the reduction of K_y due to the presence of cracks becomes less significant for c increasing. However, in case of gentle slopes (see Figure 9a), there is an inversion of the trend at $\phi = 30°$: for slopes with $\phi > 30°$ the reduction in K_y due to the presence of cracks becomes more significant for c increasing.

As noted in the investigation of the stability factor under prescribed seismic excitation, assuming the presence of the most unfavourable crack can be overly conservative. When the maximum depth of

DOI: 10.1002/nag

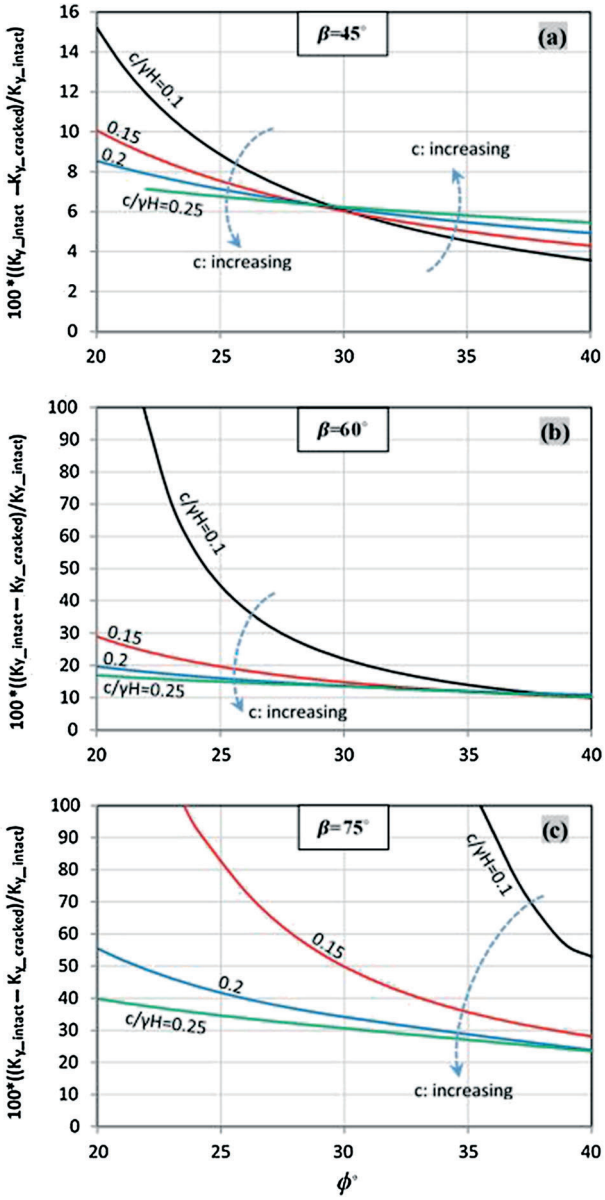

Figure 9. Percentage of reduction in the yield acceleration because of the presence of the most unfavourable crack for the stability of the slope with $\lambda = 0$. a) $\beta = 45°$, b) $\beta = 60°$ and c) $\beta = 75°$.

cracks in a slope can be inferred by either a stress analysis or in-situ measurements, this information can be included in the search for the least upper bound on K_y (problem *ii*) listed in the Introduction). Mathematically, this is done by imposing the following constraint [25]:

$$\exp[\tan\phi.\zeta]\sin\zeta = \left[\exp[\tan\phi.\chi]\sin\chi\left(1-\frac{\delta}{H}\right)+\frac{\delta}{H}\exp[\tan\phi.\upsilon]\sin\upsilon\right] \tag{6}$$

into the minimisation of $f_y(\chi, \upsilon, \zeta, \phi, \beta, c/\gamma H, \lambda)$ in Eq. (5). In Figure 10, the function $K_y^{\delta}(\delta)$ obtained from the minimisation of $f_y(\chi, \upsilon, \zeta, \phi, \beta, c/\gamma H, \lambda)$ constrained by Eq. (6) is plotted against the prescribed δ values for $\lambda = 0$, $\lambda = 0.5$ and $\lambda = 1$. $K_y^{\delta}(\delta)$ gradually decreases for δ increasing until a minimum at $\delta = \delta_{\min}$ is reached and then increases for δ increasing (see the grey curves in Figure 10). Note that the results represented by the grey curves are obtained assuming the log-spiral failure surface C-D

DOI: 10.1002/nag

constrained to depart from the crack bottom end (see Eq. (6)). When $\delta/H \to 1$, the function $K_y^{\delta}(\delta)$ tends to infinity because the volume of the wedge E-D-C-B sliding away becomes infinitesimal. However, physics dictates that the failure mechanism taking place may involve one part only of the total crack depth, i.e. the log-spiral D-C may depart from the crack above its bottom end. This possibility is not reflected by the mathematical function $K_y^{\delta}(\delta)$ because Eq (6) constrains the failure log-spiral C-D to depart from the crack bottom end. For $\delta > \delta_{\min}$, the least upper bound on the yield acceleration coefficient is provided by $K_y^{\delta}(\delta = \delta_{min})$ which is represented by black horizontal lines in Figure 10.

Finally from Figure 10 emerges that for steep slopes (Figure 10d and e), the presence of a vertical downward acceleration reduces the yield seismic coefficient (hence it is detrimental to slope stability), whereas for gentle slopes with high ϕ (Figure 10c) the opposite is true. This trend is in agreement with the results of the investigation, carried out in the previous section, on the influence of K_v on the stability factor for prescribed values of K_h.

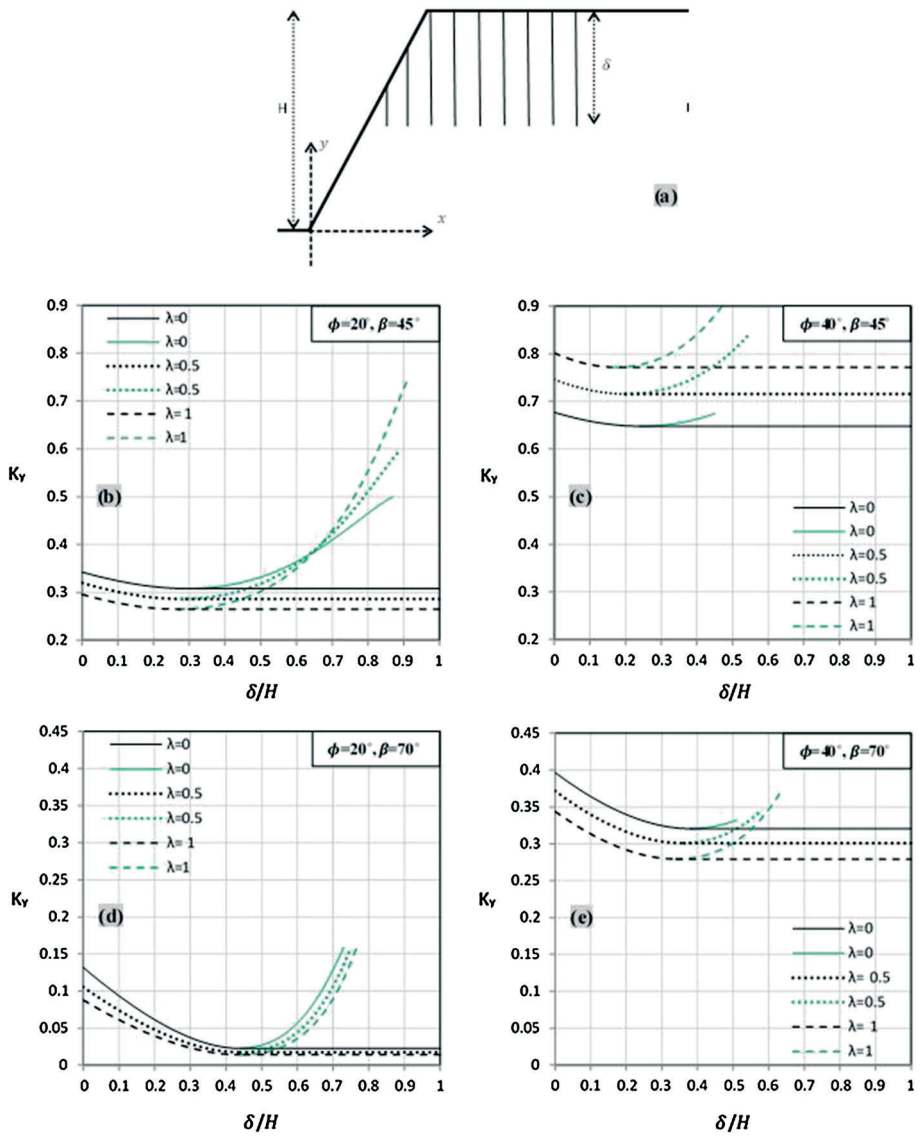

Figure 10. a) Visualisation of a slope subject to cracks of known depth but unspecified location. In b), c), d) and e) K_y is plotted against the prescribed crack depth for slopes of various β, ϕ and λ values with $c/\gamma H = 0.15$: b) $\phi = 20°$, $\beta = 45°$; c) $\phi = 40°$, $\beta = 45°$; d) $\phi = 20°$, $\beta = 70°$; e) $\phi = 40°$, $\beta = 70°$. The coloured lines represent the mathematical function $K_y^{\delta}(\delta)$, whilst the black lines represent the yield seismic coefficient of the slope.

DOI: 10.1002/nag

5. VALIDATION

The validation exercise consisted of performing FE displacement based analyses with strength reduction technique assuming an associated flow rule ($\phi = \Psi$) and FE upper and lower bound limit analyses to determine the yield seismic coefficient for a prescribed crack depth (problem *ii* in 'Introduction') and in the presence of the most unfavourable crack for the slope (problem *i*). The software package Opt+umCE [31] was used for this purpose because it allows running both types of analyses. Mesh dependency of the numerical results was checked by running simulations for different mesh sizes. The results here reported refer to simulations with a sufficient large number of elements so that mesh dependency is negligible. In Figure 11a, the yield seismic coefficient obtained for various values of prescribed crack depth is plotted. It can be noted that (our) analytical LA upper bound is significantly lower (i.e. better) than the FE upper bound. Also the gap between the numerical upper and lower bounds remains within ±9%, for any value of prescribed crack depth (the largest gap being at high depths). These results are consistent with the findings of Loukidis et al. [7] for intact slopes subject to seismic actions. Finally note that the analytical upper bounds here found are quite close to the numerical lower bounds so that true collapse values can be determined, by taking the average of the two bounds, with an accuracy of ± 3 %.

In Figure 11b, the failure mechanism obtained from FE displacement based analyses with strength reduction technique and the mechanism obtained from our analytical upper bound are plotted for the case

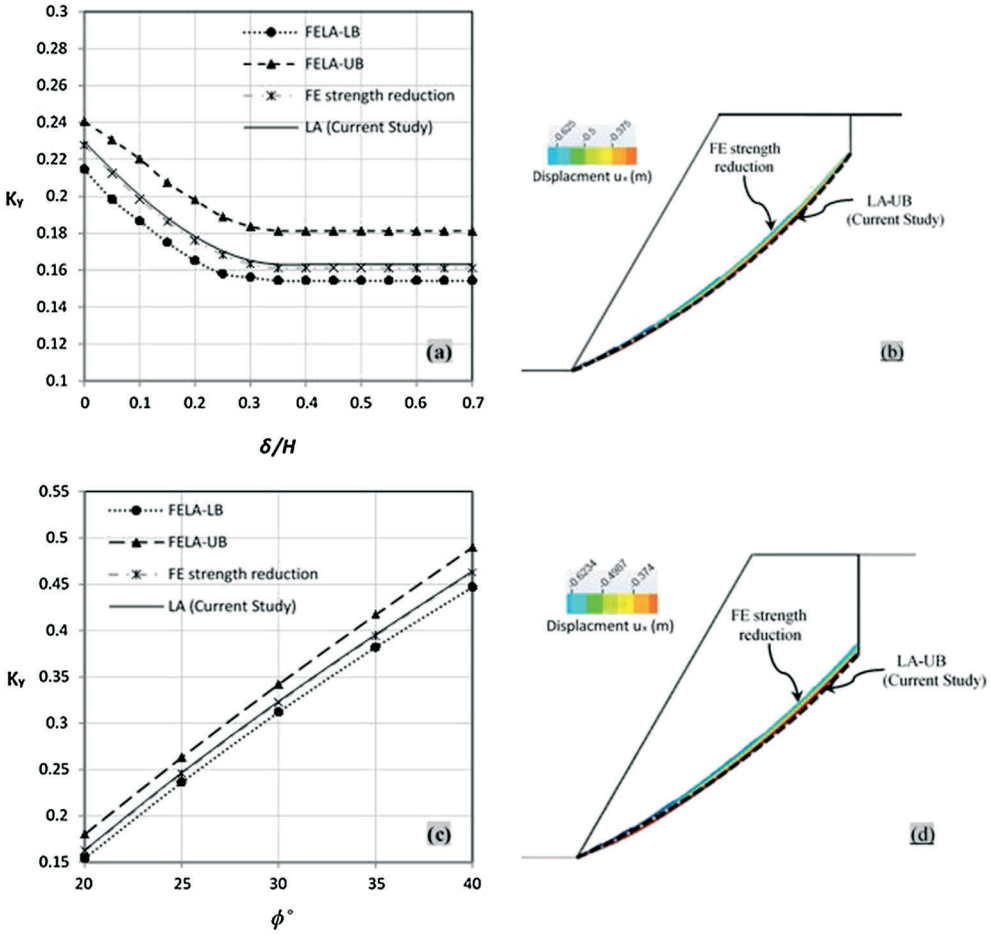

Figure 11. Comparison between the current analytical results and those obtained using finite element method (FE-limit analysis and FE-displacement-based method using strength reduction technique) for $\phi = 20°$, $\beta = 60°$ and $\lambda = 0$. (a) and (b) refer to the case of a slope subject to cracks of any possible location with a prescribed depth of $\delta/H = 0.1$. (c) and (d) refer to the same slope subject to the most unfavourable crack for its stability.

DOI: 10.1002/nag

of $\delta/H = 0.1$. A very good agreement is apparent. This implies that the failure mechanism assumed in the analyses presented in this paper, rigid rotation of block E-D-C-B, is not only a kinematically admissible mechanism, but it can also be considered a proxy of the true collapse mechanism. Therefore the failure mechanisms determined in the presented analyses can be used to obtain an estimate of the volume of the failed material especially for the central part of a 3D landslide where plane strain conditions apply. For this reason the areas of the failure mechanisms determined in this paper are provided in the 'Supporting Information'. Furthermore, several numerical analyses in the last decade for both associated and non associated geomaterials, via the finite difference method [32], via the FE method ([7], [33]; [34, 35]) and via the discrete element method [36, 37] have shown that a log-spiral rigid rotational mechanism is a realistic failure mechanism for uniform c–ϕ intact slopes under either static or seismic conditions. The validation exercise here presented extends this knowledge to slopes manifesting cracks.

In Figure 11c, the yield seismic coefficient obtained for the case of the most unfavourable crack being present is plotted for various values of ϕ. To find the yield seismic coefficient associated to the most detrimental crack scenario by the FE method is not a straightforward exercise. In fact, in principle the depth and position of the most unfavourable (critical) crack may differ from the one determined by minimisation of $f_y(\chi, \upsilon, \zeta, \varphi, \beta, c/\gamma H, \lambda)$ in Eq. (5). To find the critical crack, several analyses need to be run for the same slope, each analysis for a crack of a different prescribed depth and position. The crack associated to the mechanism giving rise to the minimum value of the yield seismic coefficient is the critical one. According to Figure 11d, the most unfavourable crack is slightly deeper but almost in the same location as the one determined by our analytical LA. Analogous results, not reported for sake of space, were obtained when the stability factor is sought rather than the yield seismic coefficient.

6. EXTENSION OF THE SLOPE ZONES UNAFFECTED BY THE PRESENCE OF CRACKS

In Utili [25], it is shown that the presence of cracks reduces the stability of a slope only if they are located in a region inside the slope, depicted in Figure 12a as extending between the horizontal coordinate x_1 and x_2. The effect of seismic acceleration on the extension of this zone is here investigated. The location of the crack needs to be prescribed by imposing the following constraint [25]:

$$\exp[\tan\phi.\chi]\sin\chi = \left[\exp[\tan\phi.\upsilon]\sin\upsilon + \frac{\exp[\tan\phi.\upsilon]\cos\upsilon - \exp[\tan\phi.\zeta]\cos\zeta}{x/H}\right] \tag{7}$$

into the minimisation of $f(\chi, \upsilon, \zeta, \phi, \beta, K_h, \lambda)$ in Eq. (5) (problem *iii* in 'Introduction'). Once the stability factors associated to failure mechanisms involving cracks of prescribed location, x, are found, i.e. the function $N(x)$, then the limits, x_1 and x_2, are determined as the values of x where $N(x) = N_{int}$ with N_{int} being the stability factor for the intact (un-cracked) slope. The obtained results are shown in Figure 12b, where the distance of the innermost limit of the 'unaffected' zone from the slope toe, x_2, is plotted for various levels of K_h. In the figure, slopes of various inclinations are considered for both cases of low and high ϕ (20° and 40° respectively). It can be observed that for a sufficiently high value of K_h, the curves relative to various slope inclinations (e.g. $\beta = 45°$; $\beta = 60°$; $\beta = 75°$) tend to intersect at a same point in all the cases analysed. This means that for a sufficiently high value of K_h, the extension of the zone where the presence of cracks affects slope stability is no longer a function of the slope inclination, but of ϕ and K_v solely. This result can be explained by looking at the geometry of the failure mechanisms taking place: for increasing K_h, the failing wedge involves an increasingly larger inward portion of slope especially along the horizontal direction, to the extent that both the area of the failing wedge (governing the amount of external work) and the length of the log-spiral failure line (governing the amount of energy dissipated) become very little affected by the inclination of the slope face.

Moreover, the influence of K_v on the extension of the zone is important: comparing the curves for the case of no vertical acceleration ($\lambda = 0$) with the curves for the case of vertical acceleration present, $\lambda = \pm 1$, a marked difference between the trends can be observed. The direction of the vertical acceleration is also important: upward acceleration ($\lambda = -1$) makes the zone where the presence of cracks affects slope stability larger (see the dotted lines in Figure 12b) whereas downward acceleration ($\lambda = +1$) reduces the extension of the zone (see the dashed lines in Figure 12b). With regard

DOI: 10.1002/nag

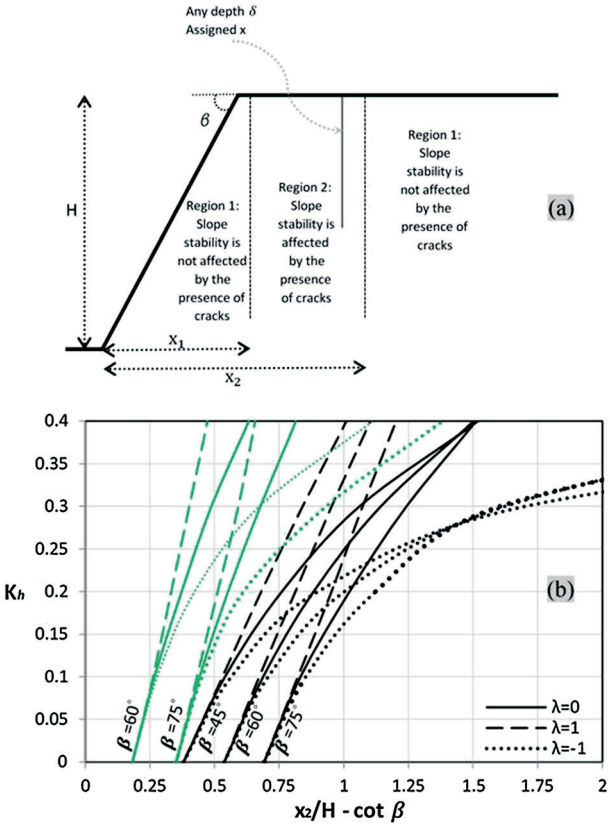

Figure 12. a) Illustration of the zones where cracks do and do not affect slope stability. b) The distance ($x_2 - \cot\beta$) is plotted against K_h for various values of λ and β. Black lines are for $\phi = 20°$ and coloured lines for $\phi = 40°$.

to ϕ, when friction is low (so cohesion tends to contribute more to the shear resistance against sliding) the zone where the presence of cracks affects slope stability is larger than when friction is high (so friction tends to contribute more to shear resistance against sliding).

7. INFLUENCE OF CRACKS ON EARTHQUAKE INDUCED DISPLACEMENTS

The derivation of an analytical expression to calculate permanent seismic induced displacements for intact slopes was carried out by Chang et al. [3] based on Newmark's method [24]. The presence of cracks makes the geometry of the failing wedge rotating away substantially different (see Figure 1) and, as a consequence, makes the analytical expression needed to calculate the induced displacements different too. Defining u_x, as the horizontal displacement of the slope toe, its rate can be calculated as [3]:

$$\delta u_x = r_v \sin\upsilon \delta\theta = r_v \sin\upsilon \iint_{\delta t\ \delta t} \ddot{\theta} dt\, dt = \mathrm{C} \iint_{\delta t\ \delta t} \left(K_i - K_y\right) \mathrm{g}\, dt\, dt \tag{8}$$

with $\ddot{\theta}$ being the angular acceleration of the failing wedge and C a dimensionless coefficient relating the displacement of the slope toe to the integral of the recorded earthquake acceleration above gK_y. $K_i g$ is the horizontal acceleration of the failing wedge. The seismic induced displacements can be calculated from Eq. (8). Assuming the most unfavourable crack being present in the slope, the following expression for C is found (calculations given in Appendix B):

$$\mathrm{C} = \frac{\gamma r_\chi^4 [\exp[\tan\phi(\upsilon - \chi)]\sin\upsilon] \begin{bmatrix} \lambda(f_{1\mathrm{v}} - f_{2\mathrm{v}} - f_{3\mathrm{v}} - f_{4\mathrm{v}} + f_{5\mathrm{v}} + f_{6\mathrm{v}}) + \\ (f_{1\mathrm{h}} - f_{2\mathrm{h}} - f_{3\mathrm{h}} - f_{4\mathrm{h}} + f_{5\mathrm{h}} + f_{6\mathrm{h}}) \end{bmatrix}}{Gl^2}. \tag{9}$$

DOI: 10.1002/nag

According to Eq. (9), C depends on both the slope geometrical features and the ground strength parameters. C values are plotted in Figure 13 for various combinations of K_y, β and ϕ. It is convenient to plot C as a function of K_y, β and ϕ because K_y appears explicitly in the double integral in Eq. (8), i.e. out of the four parameters $\gamma H/c$, β, ϕ and K_y, only three are independent. In Figure 13, values of C calculated for intact slopes are reported as well for sake of comparison.

To assess the influence of the presence of cracks on seismic induced displacements an example is here considered. The records of two well-monitored earthquakes, the Northridge earthquake in 1994 (California, USA) and the Loma Prieta earthquake in 1989 (California, USA), whose features are provided in Table I, are applied to a slope with $\phi = 20°$, $c/\gamma H = 0.1$, $\beta = 55°$ and $\lambda = 0$. The horizontal displacement of the slope toe accumulating over time is plotted in Figure 14a whilst the final accumulated displacement is plotted against ϕ values in Figure 14b for both cases of intact slope and slope subjected to the most unfavourable (critical) crack. By comparing the two curves for the same given earthquake, it turns out that the presence of cracks increases the amount of displacement significantly: for instance, in the case of the Northridge earthquake, cracks make the total accumulated displacement five times larger than the displacement occurring if the slope is un-fissured. With regard

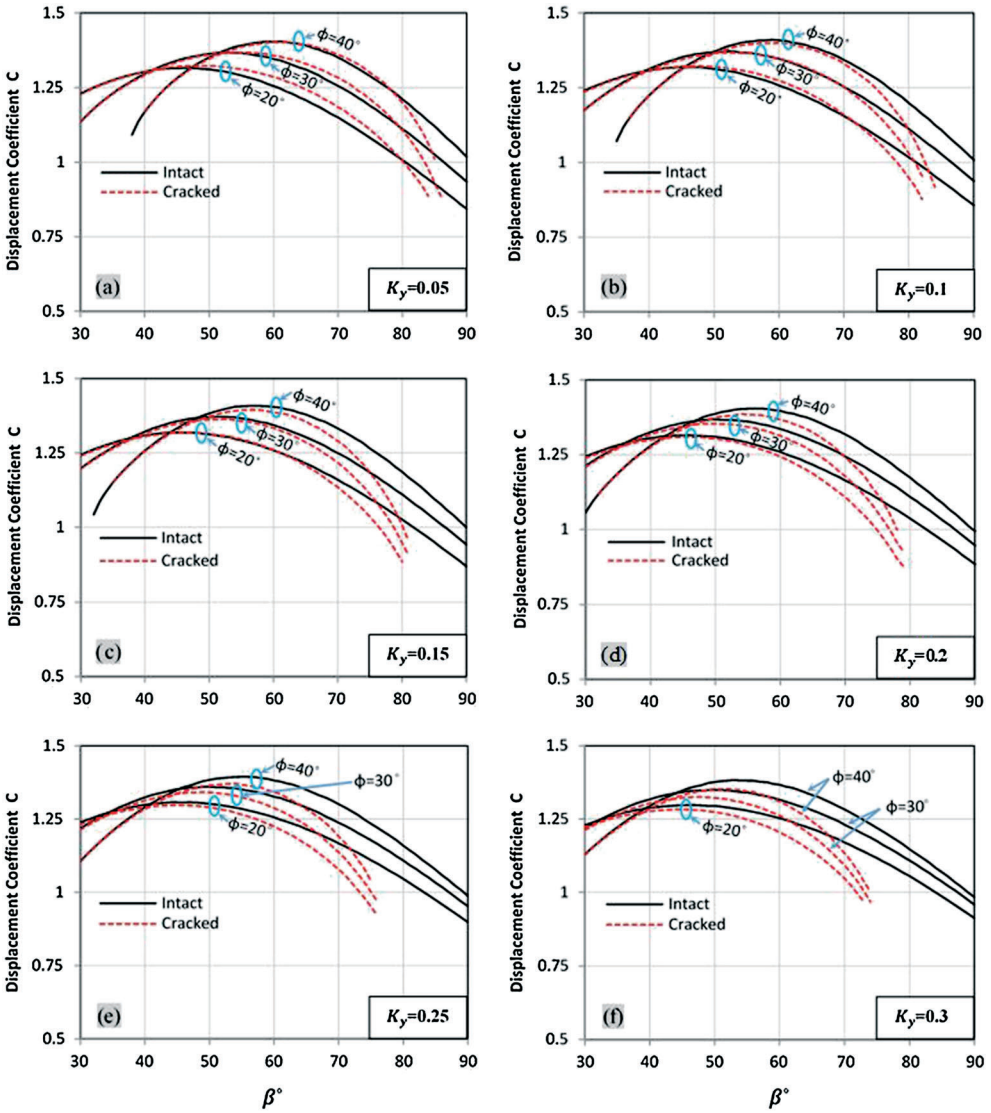

Figure 13. Seismic displacement coefficient versus slope inclination for intact slopes (solid lines) and for slopes subject to the most unfavourable crack (dashed lines) for various values of β, ϕ, and K_y.

DOI: 10.1002/nag

to the influence of the internal friction angle (ϕ), it can be observed that the difference between displacements undergone in case of intact slope and in case of fissured slope is strongly affected by the value of ϕ with the difference decreasing for increasing ϕ and becoming negligible at high ϕ.

Finally, the relationship between crack depth and final accumulated displacements was investigated by analysing an example case. Final accumulated displacements were calculated for various prescribed crack depths (δ) assuming as input the accelerogram of the Northridge earthquake and for various level of vertical acceleration (Eqs. (5), (6) and (9)). The final accumulated displacements are plotted in Figure 15 against δ/H. From the figure a highly non-linear dependence of the displacements on crack depth is apparent implying that limiting the maximum crack depth (e.g. on the slope upper surface to increase the ground tensile strength) can have a substantial beneficial effect in reducing

Table I. Main characteristics of the earthquakes considered in the example cases.

Earthquake	Northridge	Loma Prieta
Date	17/1/1994	9/2/1989
Station	24283 Moorpark—Fire Sta.	57476 Gilroy—Historic Bldg.
Magnitude	6.7	6.9
Direction	180°	180°
Peak accel. (g)	0.292	0.241
Epicentre distance (km)	23	28.1

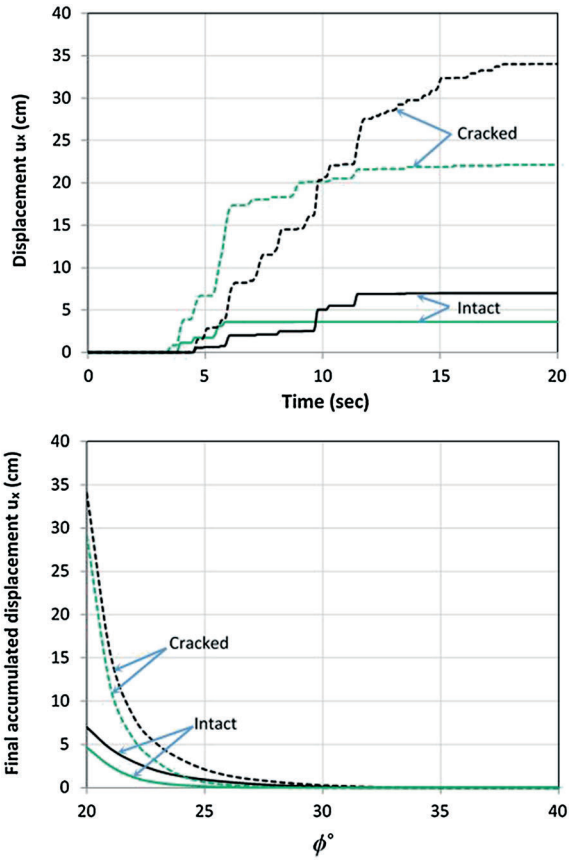

Figure 14. a) Horizontal displacement of the slope toe, u_x, versus time ($\phi = 20°$, $\beta = 55°$, $\lambda = 0$ and $c/\gamma H = 0.1$). b) Relationship between the final accumulated displacement u_x and the angle of internal friction ($\beta = 55°$, $\lambda = 0$ and $c/\gamma H = 0.1$). Black lines represent the displacements induced by the Northridge earthquake, whilst coloured lines the displacements induced by the Loma Prieta earthquake. Solid lines refer to the case of intact slope, whilst dashed lines to the case of slope subject to the most unfavourable crack.

DOI: 10.1002/nag

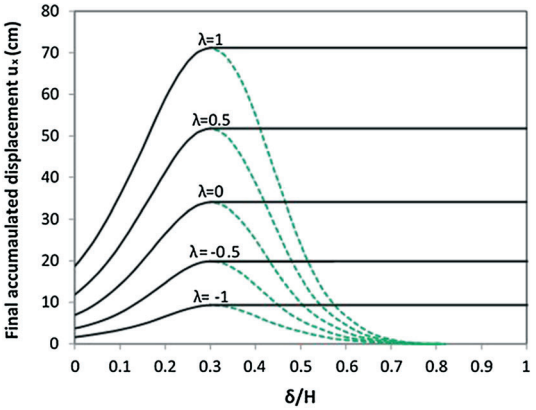

Figure 15. Horizontal final displacement at the slope toe versus normalised crack depth for a slope of given characteristic ($\phi = 20°$, $\beta = 55°$ and $c/\gamma H = 0.1$) subject to the Northridge earthquake for various values of λ.

displacements. Furthermore, Figure 15 is useful to investigate the influence of the vertical acceleration on accumulated displacements. In the case here considered, it turns out that the vertical acceleration has a significant influence with downward vertical acceleration being detrimental to slope stability and upward vertical acceleration being beneficial. However, according to the results reported in previous sections of the paper, depending on the geometrical and mechanical features of the slope (i.e. the values of ϕ and β), the opposite may also be true.

8. CONCLUSIONS

A comprehensive parametric analysis was carried out to investigate the effect of seismic action on fissured slopes employing the upper bound limit analysis method together with the pseudo static approach. An analytical solution was derived assuming uniform c, ϕ slopes with vertical cracks of either known or unknown geometry. Charts providing the stability factor for fissured slopes subject to both horizontal and vertical accelerations and charts providing the yield seismic coefficient for any combination of c, ϕ and slope face inclination were produced assuming the existence in the slope of the most unfavourable crack.

It was found that fissures may substantially reduce slope stability, i.e. lower both stability factor and yield acceleration up to 30% in comparison with the case of intact slope, with the amount of reduction depending on both the geometrical characteristics of the slope and the ground strength parameters: the reduction is higher for steep slopes of low friction angle subject to high accelerations, whereas for gentle slopes of high ϕ subject to moderate earthquakes it is negligible.

Also the effect of vertical seismic acceleration on slope stability was analysed for both cases of intact and fissured slopes. Maps showing which case is more critical for slope stability between no vertical acceleration, upward acceleration and downward acceleration were provided for any combination of β, ϕ and K_h.

Maps showing zones within the slope where cracks have no detrimental effect on its stability were provided for various combinations of horizontal and vertical acceleration. To produce the maps, the location of the cracks was prescribed in the search for the most critical failure mechanism. When the presence of one or more cracks in a slope is known, the maps tell the geotechnical engineer whether the crack may be discarded from the stability analysis and may also help inspection engineers to reduce significantly the extension of the zones in a slope or embankment to be inspected.

Finally, Newmark's approach was employed to calculate seismic induced displacements. Horizontal yield accelerations were calculated for any combination of β, ϕ and K_h of engineering interest, having assumed the most unfavourable crack for the stability of the slope to be present. Unlike Newmark's original formulation, rotational failure mechanisms, which are more critical than translational ones, were considered in the presented analysis. Seismic displacement coefficients were calculated as a function of the slope characteristics. Then, the relationship between crack depth and final accumulated displacements was investigated for an example slope subjected to the accelerograms of two past

DOI: 10.1002/nag

earthquakes. It emerges that the displacements induced for a fissured slope can be significantly larger, up to five times, than the case of intact slope depending on the slope characteristics.

NOTATION

A	area of the failing wedge
$A_1, A_2, A_3,..$ *etc.*	areas utilised in the calculation of the external work.
c	cohesion
C	seismic displacement coefficient
$f_{1v}, f_{2v}, f_{3v},..$ *etc.*	mathematical function for the external work rate done by the gravity, of the corresponding areas: A_1, A_2, etc.
$f_{1h}, f_{2h}, f_{3h},..$ *etc.*	mathematical function for the external work rate done by the horizontal seismic inertia, of the corresponding areas: A_1, A_2, etc.
f_d	function for the dissipated energy.
f_{PSh}	horizontal pseudo-static force
f_{PSv}	vertical pseudo-static force
G	weight of the failing wedge
g	gravitational acceleration
H	slope height
H_{cr}	critical slope height
K_h	horizontal seismic acceleration coefficient
K_v	vertical seismic acceleration coefficient
K_y	yield seismic acceleration coefficient
l	arm length of G
L_1, L_2	lengths defined in Figure 1
m	mass of the failing wedge
N	stability factor upper bound
N_s	stability factor
$N_\uparrow$	stability factor upper bound associated with the upward vertical acceleration
N_0	stability factor upper bound associated with nil vertical acceleration
$N_\downarrow$	stability factor upper bound associated with the downward vertical acceleration
r	generic radius of curvature of the logarithmic spiral
r_χ	minimum radius of curvature of the logarithmic spiral D-F, see Figure 1
r_υ	maximum radius of curvature of the logarithmic spiral of the failure mechanism
r_ζ	minimum radius of curvature of the logarithmic spiral of the failure mechanism
$\dot{\mathbf{u}}$	displacement rate (vector)
$\dot{W}_{ext}$	rate of external work
$\dot{W}_d$	rate of internally dissipated energy
$\dot{W}_1, \dot{W}_2, \dot{W}_3,$ .. *etc.*	external work rates of the corresponding areas: A_1, A_2, etc.
x	horizontal distance of crack from slope toe
x_c	horizontal distance of the most unfavourable crack for the stability of the slope from the slope toe
y	vertical distance from slope toe
β	Inclination of the slope front
γ	soil unit weight
δ	crack depth
δ_c	depth of the most unfavourable crack for the stability of the slope measured from the slope upper face
ζ	minimum angle of the logarithmic spiral of the failure mechanism
θ	generic angle of the logarithmic spiral
$\dot{\theta}$	angular velocity
$\ddot{\theta}$	angular acceleration
λ	ratio K_v/K_h
υ	maximum angle of the logarithmic spiral of the analysed failure mechanism

DOI: 10.1002/nag

ϕ	internal friction angle
η	angle between displacement rate, $\dot{u}$, and the crack
χ	minimum angle of the logarithmic spiral
Ψ	angle of dilation

APPENDIX A:

The rate of external work for the sliding wedge E-D-C-B, $\dot{W}_{ext}$, is calculated from the following summation:

$$\dot{W}_{ext} = \dot{W}_1 - \dot{W}_2 - \dot{W}_3 - \left(\dot{W}_4 - \dot{W}_5 - \dot{W}_6\right) \tag{A.1}$$

where $\dot{W}_1, \dot{W}_2, \dot{W}_3, \dot{W}_4, \dot{W}_5$ and $\dot{W}_6$ are the external work rates corresponding to blocks P-D-F, P-E-F, P-D-E, P-C-F, P-B-F and P-C-B respectively (see Figure 1). Their final expressions are listed as follow:

$$\begin{aligned}\dot{W}_1 &= \dot{\theta}\gamma r_\chi^3[(1+K_v)f_{1v} + K_h f_{1h}] \\ &= \dot{\theta}\gamma r_\chi^3\left[\begin{array}{c}(1+K_v)\dfrac{\exp[3\tan\phi\,(\upsilon-\chi)]\,(3\tan\phi\cos\upsilon+\sin\upsilon)-3\tan\phi\cos\chi-\sin\chi}{3\,(1+9\tan^2\phi)}+\\ K_h\dfrac{\exp[3\tan\phi\,(\upsilon-\chi)]\,(3\tan\phi\sin\upsilon+\cos\upsilon)-3\tan\phi\sin\chi+\cos\chi}{3(1+9\tan^2\phi)}\end{array}\right]\end{aligned} \tag{A.2}$$

with $\dot{\theta}$ being the rate of angular displacement of the failing wedge E-D-C-B.

$$\begin{aligned}\dot{W}_2 &= \dot{\theta}\gamma r_\chi^3[(1+K_v)f_{2v} + K_h f_{2h}] \\ &= \dot{\theta}\gamma r_\chi^3\left[(1+K_v)\frac{L_1}{6r_\chi}\sin\chi\left(2\cos\chi - \frac{L_1}{r_\chi}\right) + K_h\frac{L_1}{3r_\chi}\sin^2\chi\right]\end{aligned} \tag{A.3}$$

$$\begin{aligned}\dot{W}_3 &= \dot{\theta}\gamma r_\chi^3[(1+K_v)f_{3v} + K_h f_{3h}] \\ &= \dot{\theta}\gamma r_\chi^3\left[\begin{array}{c}\dfrac{(1+K_v)}{6}\exp[\tan\phi(\upsilon-\chi)]\left(\sin(\upsilon-\chi)-\dfrac{L_1}{r_\chi}\sin\upsilon\right)\left(\cos\chi-\dfrac{L_1}{r_\chi}+\exp[\tan\phi(\upsilon-\chi)]\cos\upsilon\right)\\ +\dfrac{K_h}{6}\exp[\tan\phi(\upsilon-\chi)]\left(\sin(\upsilon-\chi)-\dfrac{L_1}{r_\chi}\sin\upsilon\right)(\sin\chi+\exp[\tan\phi(\upsilon-\chi)]\sin\upsilon)\end{array}\right]\end{aligned} \tag{A.4}$$

$$\begin{aligned}\dot{W}_4 &= \dot{\theta}\gamma r_\chi^3[(1+K_v)f_{4v} + K_h f_{4h}] \\ &= \dot{\theta}\gamma r_\chi^3\left[\begin{array}{c}(1+K_v)\dfrac{\exp[3\tan\phi(\zeta-\chi)](3\tan\phi\cos\zeta+\sin\zeta)-3\tan\phi\cos\chi-\sin\chi}{3(1+9\tan^2\varphi)}+\\ K_h\dfrac{\exp[3\tan\phi(\zeta-\chi)](3\tan\phi\sin\zeta+\cos\zeta)-3\tan\phi\sin\chi+\cos\chi}{3(1+9\tan^2\phi)}\end{array}\right]\end{aligned} \tag{A.5}$$

$$\begin{aligned}\dot{W}_5 &= \dot{\theta}\gamma r_\chi^3[(1+K_v)f_{5v} + K_h f_{5h}] \\ &= \dot{\theta}\gamma r_\chi^3\left[(1+K_v)\frac{L_2}{6r_\chi}\sin\chi\left(2\cos\chi - \frac{L_2}{r_\chi}\right) + K_h\frac{L_2}{3r_\chi}\sin^2\chi\right]\end{aligned} \tag{A.6}$$

$$\begin{aligned}\dot{W}_6 &= \dot{\theta}\gamma r_\chi^3[(1+K_v)f_{6v} + K_h f_{6h}] \\ &= \dot{\theta}\gamma r_\chi^3\left[\begin{array}{c}\dfrac{(1+K_v)}{3}\exp[2\tan\phi(\zeta-\chi)]\cos^2\zeta(\exp[\tan\phi(\zeta-\chi)]\sin\zeta-\sin\chi)\\ +\dfrac{K_h}{6}\exp[\tan\phi(\zeta-\chi)]\cos\zeta\left(\exp[2\tan\phi(\zeta-\chi)]\sin^2\zeta-\sin^2\chi\right)\end{array}\right]\end{aligned} \tag{A.7}$$

DOI: 10.1002/nag

APPENDIX B: In the following the calculations for the weight of the sliding mass E-D-C-B and its arm length, called G and l respectively, are detailed:

$$G = \gamma A \tag{B.1}$$

$$\text{with } A = A_1 - A_2 - A_3 - A_4 + A_5 + A_6$$

$$A_1 = \frac{r_\chi^2}{2}\left[\frac{\exp[2\tan\phi(\upsilon - \chi)] - 1}{2\tan\phi}\right] \tag{B.2}$$

$$A_2 = \frac{1}{2} r_\chi L_1 \sin\chi \tag{B.3}$$

$$A_3 = \frac{1}{2} r_\chi H\left[\frac{\exp[\tan\phi(\upsilon - \chi)]\sin(\beta + \upsilon)}{\sin\beta}\right] \tag{B.4}$$

$$A_4 = \frac{r_\chi^2}{2}\left[\frac{\exp[2\tan\varphi(\zeta - \chi)] - 1}{2\tan\phi}\right] \tag{B.5}$$

$$A_5 = \frac{1}{2} r_\chi L_2 \sin\chi \tag{B.6}$$

$$A_6 = \frac{1}{2}\delta r_\zeta \cos\zeta = \frac{1}{2} r_\chi \delta[\exp[\tan\phi(\zeta - \chi)]\cos\zeta]. \tag{B.7}$$

The arm length l, is given by:

$$l = \sqrt{\frac{\left(\gamma r_\chi^3 (f_{1v} - f_{2v} - f_{3v} - f_{4v} + f_{5v} + f_{6v})\right)^2 + \left(\gamma r_\chi^3 (f_{1h} - f_{2h} - f_{3h} - f_{4h} + f_{5h} + f_{6h})\right)^2}{G}}. \tag{B.8}$$

ACKNOWLEDGEMENTS

The research carried out in this paper was funded by the Higher Committee for Education Development in Iraq (HCED) and H2020 Marie Skłodowska-Curie Actions RISE 2014 'Geo-ramp' grant number 645665.

REFERENCES

1. Terzaghi K. *Theoretical Soil Mechanics*. John Wiley & Sons: New York, USA, 1943.
2. Cao J, Zaman MM. Analytical method for analysis of slope stability. *International Journal for Numerical and Analytical Methods in Geomechanics* 1999; **23**(5):439–449.
3. Chang CJ, Chen WF, Yao JP. Seismic displacements in slopes by limit analysis. *Journal of Geotechnical Engineering* 1984; **110**(7):860–874.
4. Chen WF, Liu XL. *Limit Analysis in Soil Mechanics*. Elsevier: Amsterdam, Netherlands, 1990.
5. Crespellani T, Madiai C, Vannucchi G. Earthquake destructiveness potential factor and slope stability. *Geotechnique* 1998; **48**(3):411–419.
6. Gao Y, Zhang F, Lei GH, Li D, Wu Y, Zhang N. Stability charts for 3D failures of homogeneous slopes. *Journal of Geotechnical and Geoenvironmental Engineering* 2013; **139**(9):1528–1538.
7. Loukidis D, Bandini P, Salgado R. Stability of seismically loaded slopes using limit analysis. *Geotechnique* 2003; **53**(5):463–479.
8. Yang XG, Chi SC. Seismic stability of earth-rock dams using finite element limit analysis. *Soil Dynamics and Earthquake Engineering* 2014; **64**:1–10.

DOI: 10.1002/nag

9. You L, Michalowski RL. Displacement charts for slopes subjected to seismic loads. *Computers and Geotechnics* 1999; **25**(1):45–55.
10. Terzaghi K 1950. Mechanisms of Landslides. Engineering Geology (Berkeley) Volume, Geological Society of America, Boulder, CO (USA), pp. 83–123.
11. Taylor DW. *Fundamentals of Soil Mechanics*. John Wiley & Sons: New York, USA, 1948.
12. Chen WF. *Limit Analysis and Soil Plasticity*. Elsevier: Amsterdam, Netherlands, 1975.
13. Antao AN, Costa Guerra NM, Fernandes MM, Cardoso AS. Influence of tension cut-off on the stability of anchored concrete soldier-pile walls in clay. *Canadian Geotechnical Journal* 2008; **45**(7):1036–1044.
14. Baker R. Sufficient conditions for existence of physically significant solutions in limiting equilibrium slope stability analysis. *International Journal of Solids and Structures* 2003; **40**(13–14):3717–3735.
15. Vanicek I, Vanicek M. *Earth Structures in Transport, Water and Environmental Engineering*. Springer: Prague, 2008.
16. Konrad JM, Ayad R. An idealized framework for the analysis of cohesive soils undergoing desiccation. *Canadian Geotechnical Journal* 1997; **34**(4):477–488.
17. Dyer M, Utili S, Zielinski M. Field survey of desiccation fissuring of flood embankment. *Proceedings of the ICE-Water Management* 2009; **162**(3):221–232.
18. Tang CS, Cui YJ, Tang AM, Shi B. Experiment evidence on the temperature dependence of desiccation cracking behavior of clayey soils. *Engineering Geology* 2009; **114**(3-4):261–266.
19. Tang CS, Cui YJ, Shi B, Tang AM, Liu C. Desiccation and cracking behavior of clay layer from slurry state under wetting–drying cycles. *Geoderma* 2011; **166**(1):111–118.
20. Utili S, Castellanza R, Galli A, Sentenac P. Novel approach for health monitoring of earthen embankments. *Journal of Geotechnical and Geoenvironmental Engineering, ASCE* 2015; **141**(3):04014111. doi:10.1061/(ASCE)GT.1943-5606.0001215.
21. Hales TC, Roering JJ. Climatic controls on frost cracking and implications for the evolution of bedrock landscapes. *Journal of Geophysics Research: Earth Surface (2003-2012)* 2007; **112**(F2). doi:10.1029/2006JF000616.
22. Allsop W, Kortenhaus A, Morris M, Buijs F, Hassan R, Young M, Doorn N, der Meer J, Van Gelder P, Dyer M, Redaelli M, Utili S, Visser P, Bettess R, Lesniewska D, and Horst W 2007. Failure mechanisms for flood defence structures. EU FP7 FLOODSite task 4, Research Report: T04-06-01.
23. Environment Agency. 2006. Condition assessment manual. Report DR 166_03_SD01.
24. Newmark NM. Effect of earthquakes on dams and embankments. *Geotechnique* 1965; **15**(2):139–159.
25. Utili S. Investigation by limit analysis on the stability of slopes with cracks. *Geotechnique* 2013; **63**(2):140–154.
26. Michalowski RL. Stability assessment of slopes with cracks using limit analysis. *Canadian Geotechnical Journal* 2013; **50**(10):1011–1021.
27. Utili S, Crosta GB. Modeling the evolution of natural cliffs subject to weathering: 1. Limit analysis approach. *Journal of Geophysics Research: Earth Surface* 2011; **116**:F01016. doi:10.1029/2009JF001557.
28. Utili S, Nova R. On the optimal profile of a slope. *Soils and Foundations* 2007; **47**(4):717–729.
29. Ling HI, Leshchinsky D, Mohri Y. Soil slopes under combined horizontal and vertical seismic acceleration. *Earthquake Engineering & Structural Dynamics* 1997; **26**(12):1231–1241.
30. Shukha R, Baker R. Design implications of the vertical pseudo-static coefficient in slope analysis. *Computers and Geotechnics* 2008; **35**(1):86–96.
31. Optumce, (2014). OptumG2 (Version 1.14) [Computer programme] Available at www.optumce.com.
32. Dawson EM, Roth WH, Drescher A. Slope stability analysis by strength reduction. *Geotechnique* 1999; **49**(6):835–840.
33. Zheng H, Liu DF, Li CG. Slope stability analysis based on elasto-plastic finite element method. *International Journal for Numerical Methods in Engineering* 2005; **64**(14):1871–1888.
34. Conte E, Silvestri F, Troncone A. Stability analysis of slopes in soils with strain-softening behaviour. *Computers and Geotechnics* 2010; **37**(5):710–722.
35. Crosta GB, Utili S, Blasi D, Castellanza R. Reassessing rock mass properties and slopes instability triggering conditions in Valles Marineris, Mars. *Earth and Planetary Science Letters* 2014; **388**:329–342.
36. Utili S, Nova R. DEM analysis of bonded granular geomaterials. *International Journal for Numerical and Analytical Methods in Geomechanics* 2008; **32**(17):1997–2031.
37. Utili S, Crosta GB. Modelling the evolution of natural slopes subject to weathering part II. Discrete Element Approach. *Journal of Geophysical Research: Earth Surface* 2011; **116**:F01017.

SUPPORTING INFORMATION

Additional supporting information may be found in the online version of this article at the publisher's web site.

DOI: 10.1002/nag